Atmospheric Research 101 (2011) 595–610

Contents lists available at ScienceDirect

Atmospheric Research

journal homepage: www.elsevier.com/locate/atmos

Orographic effects on localized heavy rainfall events over southwestern Taiwan on 27 and 28 June 2008 during the post-Mei-Yu period

Ching-Sen Chen [a,*], Yuh-Lang Lin [b], Nai-Ning Hsu [a], Che-Ling Liu [a], Chih-Ying Chen [a]

[a] Institute of Atmospheric Physics, National Central University, Chung-Li 320, Taiwan
[b] Department of Physics and Department of Energy and Environmental System, NC A&T State University, Greensboro, NC 27411, USA

ARTICLE INFO

Article history:
Received 17 November 2010
Received in revised form 8 April 2011
Accepted 8 April 2011

Keywords:
Orographic effects
Localized heavy rainfall
Orographic rainfall
Mei-Yu, Taiwan

ABSTRACT

This study aims to perform observational data analyses, including European Centre for Medium-Range Weather Forecasts data, radar reflectivity, rainfall data, and numerical simulations with the Weather Research and Forecasting model to examine the orographic effects on a localized heavy rainfall episode which produced up to 204 and 161.5 mm over southwestern Taiwan on 27 and 28 June 2008, respectively. We found that the continuous inland-transport of moist air or inland-movement of convection from the nearby ocean to southwestern Taiwan occur on both days. The orographic lifting on the moist air and convection generates heavy rainfall over sloped areas on 27 June when the relatively fast southwesterly low-level wind prevails (~10 m s^{-1}). The cool air near the foothill facilitates the new development of convection on the upstream side of the old convection over the slope and produces heavy rainfall over lowlands near the foothill. On 28 June, the convection, which is embedded in a relatively slow southwesterly moist airflow, is enhanced over the low-level convergence areas in the lowlands due to the prevailing southwesterly wind. This wind is deflected by the orographic effect and produces heavy rainfall. In addition, the cool air from sloped areas enhances the offshore flow which interacts with the prevailing wind to strengthen the low-level convergence over lowlands and coasts.

1. Introduction

After the cessation of Mei-Yu season (mid-May to mid-June), which is one of the major rainfall periods in Taiwan (Chen and Chen, 2003) rainfall declines quite rapidly in late June (16 to 30 June) because the development of baroclinic disturbances and mesoscale convective systems are suppressed by the intrusion of the ridge of western Pacific subtropical high (Chen and Chen, 2003). Heavy rainfall events over southwestern Taiwan (south of 23.5°N and west of Central Mountain Range (CMR)) (Fig. 1) become less common in late June than the period of Mei-Yu season (Chen et al., 2007). Heavy rainfall here is defined as a daily rainfall accumulation greater than 130 mm and an hourly rainfall rate exceeding 15 mm recorded at a minimum of one rainfall observation site (Wang et al., 1985). This criterion of heavy rainfall is used by the forecasters of the Central Weather Bureau (CWB) of Taiwan. Xu et al. (2009) found that the extremely intense convection is present over southern Taiwan during post-Mei-Yu season from TRMM observations (their Fig. 9d). During late June in the period of 1997–2009, the annually averaged number of heavy rainfall occurrences over southwestern Taiwan is about 8.8 (Hsu, 2010). However, Hsu (2010) also showed that there were 55 heavy rainfall occurrences during late June 2008 alone. In particular, on June 27 and 28, 2008, the heavy rainfall occurrences were 10 and 4, respectively, which are significantly more frequent than the annual average. In the event of June 27, continuous rainfall appears over southwestern Taiwan with high accumulated rainfall over the lowlands

* Corresponding author. Tel.: +886 3 4220270; fax: +886 3 4256841.
E-mail address: tchencs@atm.ncu.edu.tw (C.-S. Chen).

0169-8095/$ – see front matter © 2011 Elsevier B.V. All rights reserved.
doi:10.1016/j.atmosres.2011.04.004

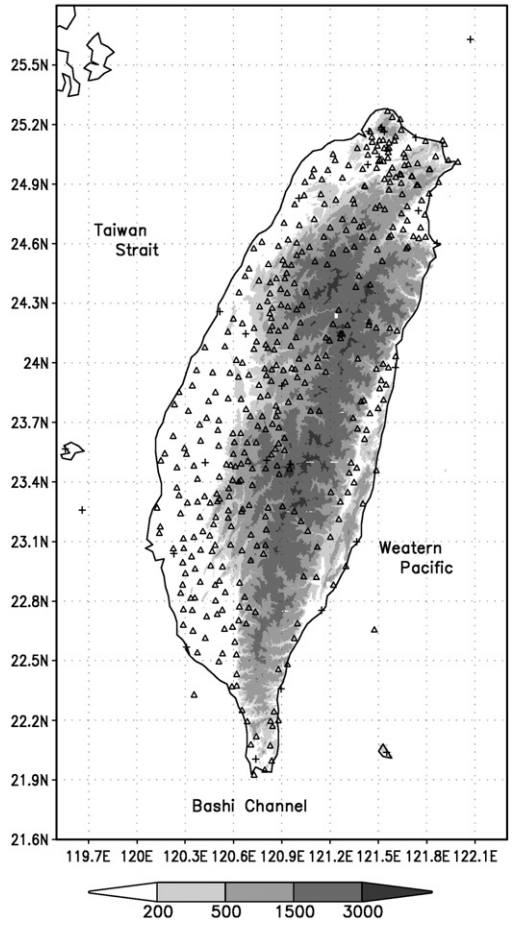

Fig. 1. Distribution of rainfall stations in Taiwan from the Automatic Rainfall and Meteorological Telemetry System (ARMTS, triangles) and twenty-five conventional stations (crosses). The gray scale shows terrain elevations in meters.

near sloped areas and mountain slopes during the period from 0900 to 1600 LST (Local Standard Time = UTC + 8 h) and produced 204 mm of maximum accumulated rainfall over sloped areas (Fig. 2). These data are obtained from 397 Automatic Rainfall and Meteorological Telemetry System (Chen et al., 2007). In the event of June 28, most of the rainfall appear over lowland areas near coasts from 0900 to 1600 LST and the maximum accumulated rainfall is 162 mm over lowland areas (Fig. 3). The occurrences of localized heavy rainfall over either sloped areas or lowland areas present a difficult, yet important, challenge to skillful weather forecasters.

Since the preferable large-scale conditions for the development of mesoscale convective systems (MCSs) and Mei-Yu fronts (Chen and Li, 1995) that are responsible for producing the majority of heavy rainfall events in Mei-Yu season (Chen and Chen, 2003; Chen et al., 2005, 2007, 2010a; Zhang et al., 2003) are not frequently present during the post-Mei-Yu period, orographic effects become relatively important for generating or enhancing heavy rainfall over southwestern Taiwan (Lin et al., 2001; Kerns et al., 2010) because approximately two-thirds of Taiwan is covered by the mountains (Fig. 1). Recently, Chen et al. (2010b) demonstrate the importance of orographic effects on the generation and maintenance of a localized heavy rainfall event in northern Taiwan on the downwind side of Taiwan's CMR in late June during the monsoon break (post-Mei-Yu periods). Over Peninsular Malaysia in Southeast Asia, the collision of the sea breeze with lee waves, gap winds and edge winds of the mountain range enhanced the convective activity on 10 June 2007 (Sow et al., 2011). Less rainfall occurs on the leeward side of Truong Son Range in central Vietnam (Yen et al., 2011). Over complex terrain like southern Italy, orographic effects are also important for regulating the total precipitation (Federico et al., 2009). Furthermore, Mastrangelo et al. (in press) shows that orographic lifting is the main mechanism for producing a heavy rainfall event over southeastern Italy on 12 November 2004.

Over southwestern Taiwan on the upwind side of the CMR under the southwesterly monsoonal flow, there have been relatively few studies of orographic effects on the generation and maintenance of localized heavy rainfall events in the monsoon break. Because the low-level prevailing southwesterly wind in late June 2008 is around 7.5 m s^{-1} (Hsu, 2010), the Froude number (Fr = U/Nh, Hunt and Snyder, 1980; also see Lin, 2007) is about 0.3, where U (wind speed) ~ 7.5 m s^{-1}, N (Brunt-Väsälä frequency) ~ 0.01 s^{-1}, and h (CMR height) ~ 2.5 km. Under such a low Fr regime, the flow convergence induced by the deflection of prevailing southwesterly winds due to orographic blocking over the windward side may generate and/or enhance heavy rainfall is well known (Lin, 2007). Near the southern peninsula of Taiwan, the peak of terrain is about 2 km (Fig. 1) and the Fr reaches a value of ~0.38. Under such a low-Froude-number regime, orographically induced mesoscale convective cells tend to propagate downstream while the entire mesoscale convective system tends to propagate upstream to be over the lower sloped areas, as demonstrated in Regime I of Chu and Lin (2000). We hypothesize that the localized heavy rainfall over sloped areas on June 27 is caused by the inland movement of the existing convection from the nearby ocean embedded in a relatively fast moist southwesterly wind being enhanced by orographic lifting over sloped areas in southern Taiwan. The rainfall evaporative cooling over the lowlands near sloped areas may facilitate the maintenance of heavy rainfall over lowlands. On June 28, the enhancement of the existing convection is embedded in a relatively slower moist southwesterly flow from the nearby ocean. This occurs in locations over low-level convergence in the lowlands due to orographically deflected prevailing southwesterly flow that may facilitate heavy rainfall. In addition, the cool air from sloped areas may enhance the offshore flow which interacts with the prevailing wind to strengthen low-level convergence over lowlands and coastal areas (Chen et al., 2005, 2010a; Kerns et al., 2010).

The objective of this study is to perform observational analyses of the European Centre for Medium-Range Weather Forecasts (ECMWF) data, satellite imagery, radar reflectivity, and rainfall data for the synoptic and mesoscale processes to examine the importance of the above two mechanisms. The mesoscale process associated with the development of the heavy rainfall event and the orographic effects on the generation/enhancement of rainfall are examined by the

Weather Research and Forecasting (WRF, Skamarock et al., 2005) model. Observational analysis will be presented in Section 2, while the numerical simulations will be presented in Section 3. In Section 4, we will discuss the formation and maintenance mechanism of the localized heavy rainfall episode. In Section 5, several sensitivity tests are performed and their results are discussed. A summary is presented in Section 6.

2. Observational analysis

2.1. Description of the dataset

Several observational datasets are used to characterize the heavy rainfall episode observed over southwestern Taiwan and to initialize and verify the results of WRF model in this study. The datasets used are: (1) ECMWF/Tropical Ocean Global Atmosphere (TOGA) data utilizing $1.125° \times 1.125°$ latitude–longitude grid spacing and 6 h time interval for the initialization of the WRF model. (2) Radar images with 2-km grid spacing from the Chigu radar of the Central Weather Bureau (CWB) of Taiwan, which are available every half an hour. The images of the maximum reflectivity (in dBZ) in the vertical column are used to trace the most intense convective systems over the southern Taiwan Strait and southwestern Taiwan. (3) Hourly rainfall data from 397 ARMTS (Chen et al., 2007) around Taiwan (Fig. 1) are used to examine the spatial and temporal characteristics of the observed rainfall.

2.2. Synoptic overview

At 0800 LST 27 June, a trough stretched from the low pressure center over Mongolia southwestward to central China (Fig. 4a). To the southeast of the China coast, Taiwan was located along the western boundary of the western Pacific subtropical high. There was no pronounced upper-level divergence over Taiwan as found in some heavy rainfall events during Mei-Yu season (Chen and Li, 1995; Chen et al., 2010a). A 500-hPa short wave trough (Hsu, 2010) was above an 850-hPa low pressure center located over southeast China (Fig. 4b). Strong southwesterly winds (~10 m s^{-1}) with high equivalent potential temperature (θ_e) prevailed over northeastern South China Sea and southern Taiwan Strait. At 0200 LST 28 June, the 300-hPa trough over central China migrated eastward without pronounced upper-level divergence near Taiwan (Hsu, 2010). Meanwhile, the 850-hPa low pressure moved northeastward to the east China coast resulting in a decrease of southwesterly winds (about 7.5 m s^{-1}, Fig. 5) over southern Taiwan Strait and northeastern South China Sea.

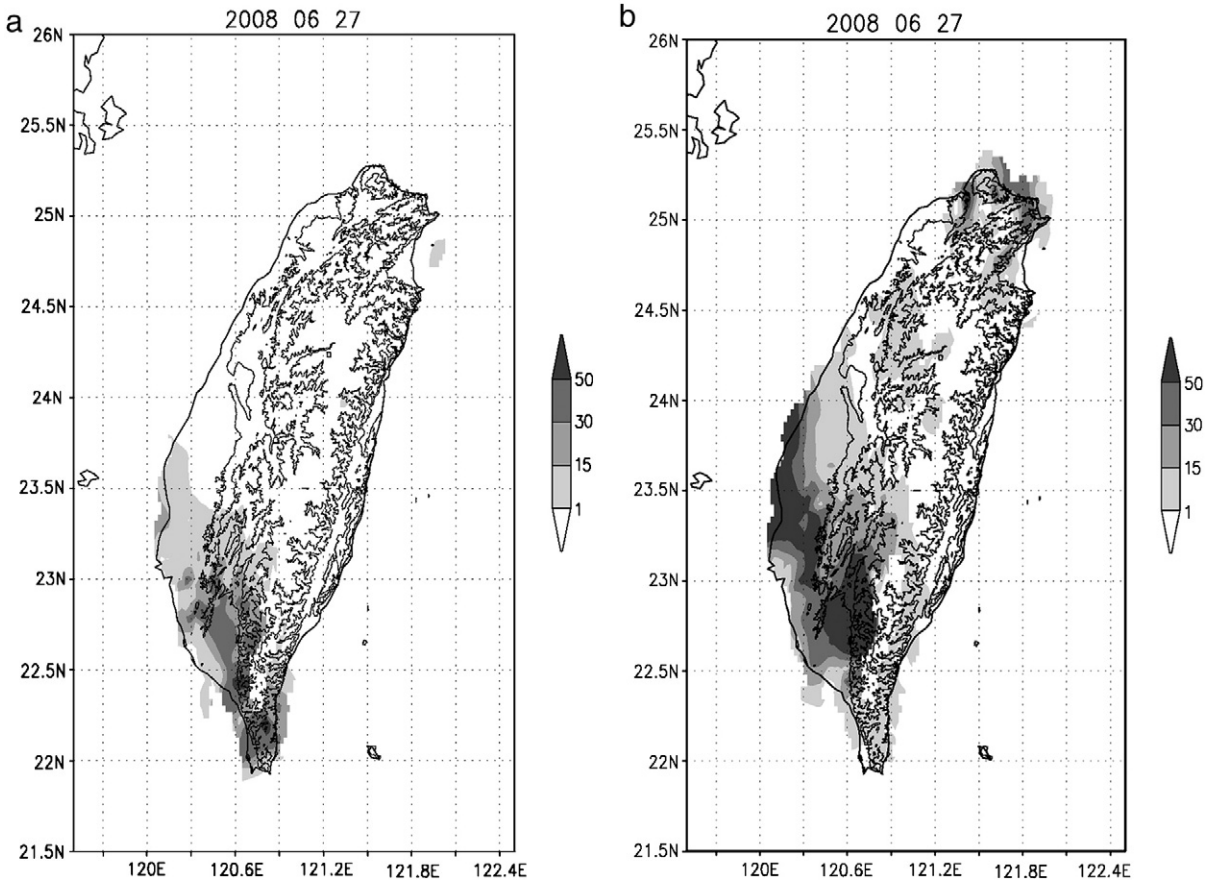

Fig. 2. (a) Accumulated rainfall during 0100–0800 LST on 27 June 2008. The magnitude is shown by the gray scale in mm. Terrain height (solid lines) is 100, 500, and 1500 m, respectively. (b) Same as (a) but for 0900–1600 LST. (c) The accumulated daily rainfall on 27 June 2008. The magnitude is shown by the gray scale in mm. The terrain elevation (solid lines) is 100, 500, and 1500 m, respectively.

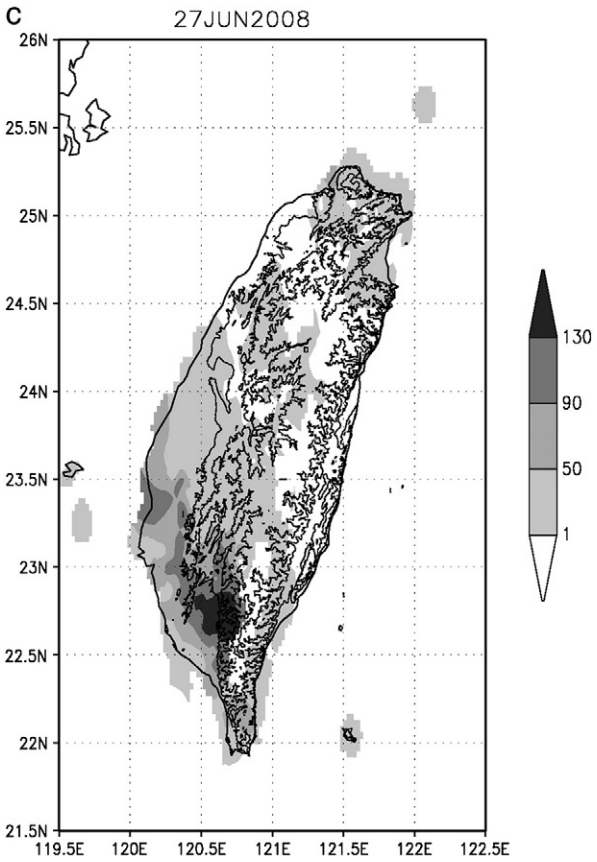

Fig. 2 (*continued*).

Fig. 5 shows the temporal change of the profiles of the wind, relative humidity, and saturated equivalent potential temperature (θ_e^*) near the northeast South China Sea just upstream of southwestern Taiwan, which occurred before and during the localized heavy rainfall episode. Prior to 0800 LST 27 June, strong low-level southwesterly winds (~10 m s^{-1}) prevailed over the northeast South China Sea accompanying the possible existence of conditional instability, which existed below 700 hPa (where $\partial\theta_e^*/\partial z<0$). The level of free convection (LFC) in the early morning over the northeast South China Sea was about 1.2 km which can be easily reached under moderate orographic lifting. Strong low-level winds continued from the morning to afternoon of 27 June in conjunction with moist air thus providing a favorable condition for generating long duration of rainfall over sloped areas. The low-level moisture decreased in the evening and then increased significantly in the early morning on 28 June resulting in a low LFC (~0.8 km). Meanwhile, the low-level wind slowed down and produced a lower-Fr regime in southern Taiwan. In this flow regime, the low-level convergence in a very moist environment over the lowland areas on the windward side of southwestern Taiwan facilitated the formation of rainfall in the lowland areas.

2.3. Convection over the southern Taiwan Strait and southwestern Taiwan

The convective activity had already appeared over northeastern South China Sea and southern Taiwan Strait in the early morning of 27 June and moved toward southwestern Taiwan (Hsu, 2010). By 0806 LST 27 June, radar echoes exceeding 45 dBZ were over the nearby ocean and the slopes of southwestern Taiwan (Fig. 6a) and produced high accumulated rainfall in mountainous areas in a few hours (Fig. 2b). The continuous inland movement of radar echoes from the nearby ocean to southwestern Taiwan is associated with persistent rainfall in sloped areas (Fig. 2). High accumulated rainfall over western coastal areas in Fig. 2b was evidenced by the inland-movement of radar echoes over southern Taiwan Strait (Fig. 6a). Rainfall decreased after 2000 LST due to the cessation of the inland-movement of convective activity from the nearby ocean (not shown). At 0230 LST 28 June, as moisture increased (Fig. 5) and some convective activity appeared above the nearby ocean closed to southwest Taiwan (Hsu, 2010) resulting in early rainfall over coastal and lowland areas (Fig. 3a). By 0806 LST, radar echoes exceeding 45 dBZ appeared over coastal and lowland areas of southwestern Taiwan (Fig. 6b) and lasted for several hours (not shown) causing high rainfall (Fig. 3b). As a result, high accumulated rainfall occurred in the morning of 28 June (Fig. 3).

It appears that the localized heavy rainfall over the slopes on June 27 (Fig. 2) was produced by orographic lifting of a relatively fast-moving moist airstream (Fig. 5) which satisfied two common ingredients (the presence of steep orography and a high moisture flow upstream) for heavy orographic rainfall (Lin et al., 2001). The rainfall over the lowlands near the coastal area on 28 June was enhanced by the interaction between the offshore flow deflected from the prevailing winds by orographic effects and prevailing monsoonal flow similar to that found in Chen et al. (2010a). Over southwestern Taiwan, southwesterly onshore flow was observed over the coastal areas of the island at 0800 and an easterly offshore flow was observed at plains stations near 23°N and southwestern slopes (Fig. 3d). The convergence, associated with the onshore flow and the offshore flow caused by orographic blocking, as well as differential heating associated with the land–sea temperature contrast likely enhanced the rainfall in the plains and coastal areas (Fig. 3c).

In summary, the above observational analysis shows that the localized heavy rainfall episode over southwestern Taiwan on 27 and 28 June 2008 was initiated by the inland movement of convective activity from the northeast South China Sea and intensified by the orographic effects.

3. Numerical simulations

3.1. Numerical experiment design

The WRF-v2 model was employed to help understand the details of the dynamics and physical processes responsible for

Fig. 3. (a) Same as Fig. 2a but for 28 June 2008. (b) Same as Fig. 2b but for 28 June 2008. (c) Same as Fig. 2c but for 28 June 2008. (d) Surface winds and virtual potential temperature (K) at 0800 LST on 28 June 2008. A full barb and a half barb represent 5 and 2.5 m s^{-1}, respectively. The terrain elevation (solid lines) is 100, 500, and 1500 m, respectively.

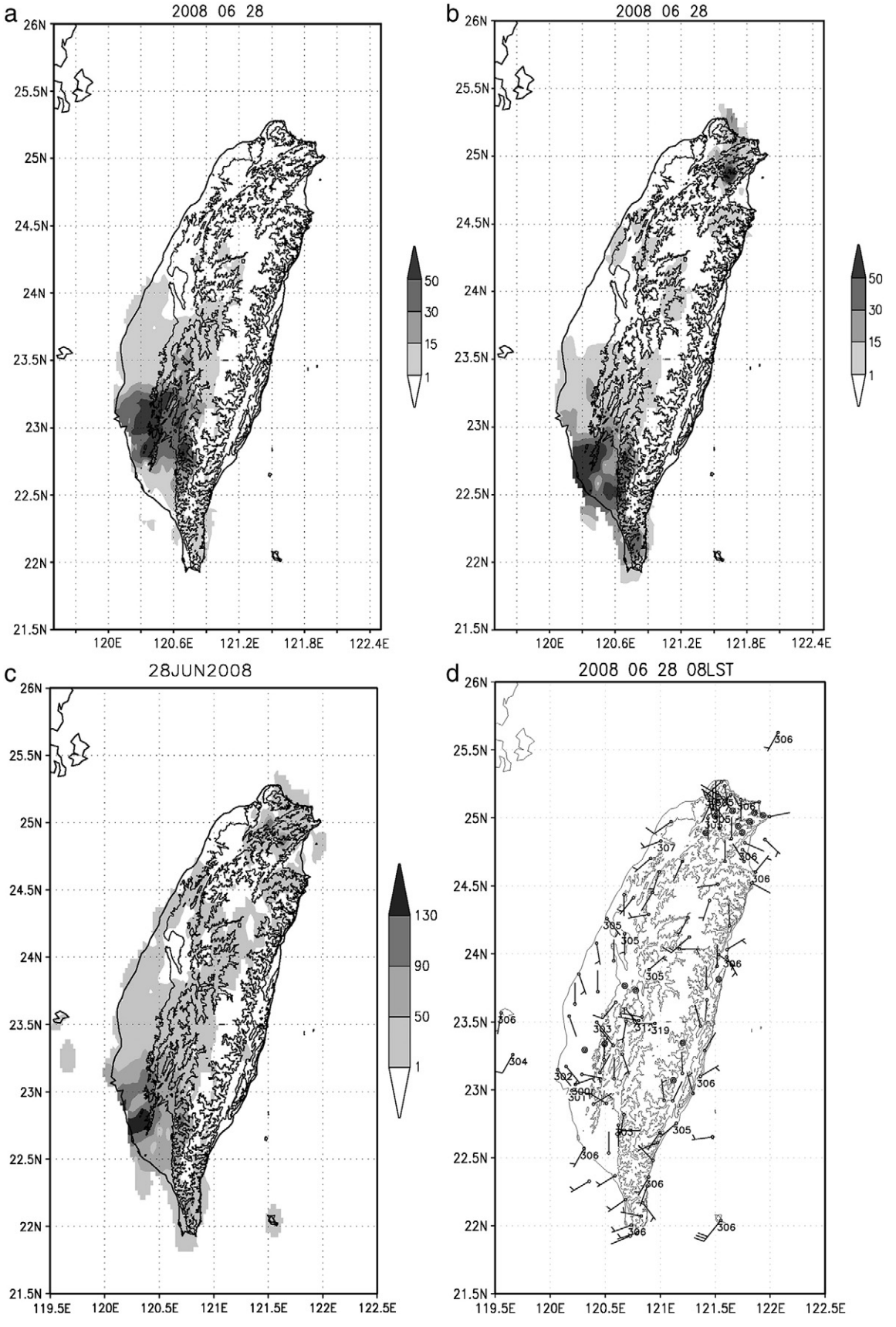
a
2008 06 28
26N
25.5N
25N
24.5N
24N
23.5N
23N
22.5N
22N
21.5N
120E
120.6E
121.2E
121.8E
122.4E
50
30
15
1
b
2008 06 28
c
28JUN2008
119.5E
120E
120.5E
121E
121.5E
122E
122.5E
130
90
50
1
d
2008 06 28 08LST

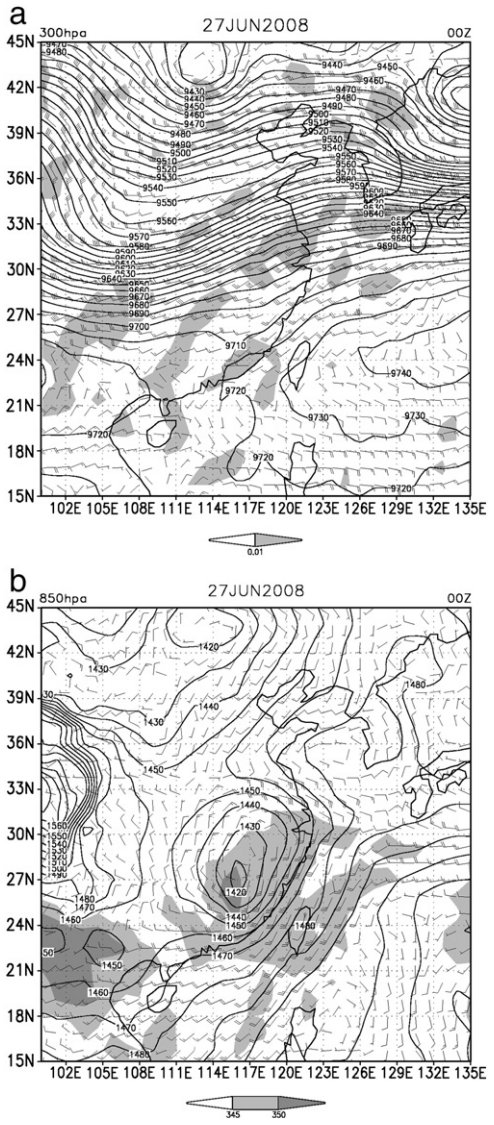

Fig. 4. (a) The 300 hPa synoptic analysis at 0800 LST 27 June 2008 from the ECMWF/TOGA data including heights (solid lines, 30 gpm contour interval) and winds (a full barb and a half barb represent 5 and 2.5 m s^{-1}, respectively; also used for other figures). The shaded areas represent divergence greater than 10^{-6} s^{-1}. (b) The 850 hPa synoptic analysis at 0800 LST 27 June 2008 from the ECMWF/TOGA data including heights (solid lines, 15 gpm contour interval) and winds. The equivalent potential temperature (K) is represented by gray scale.

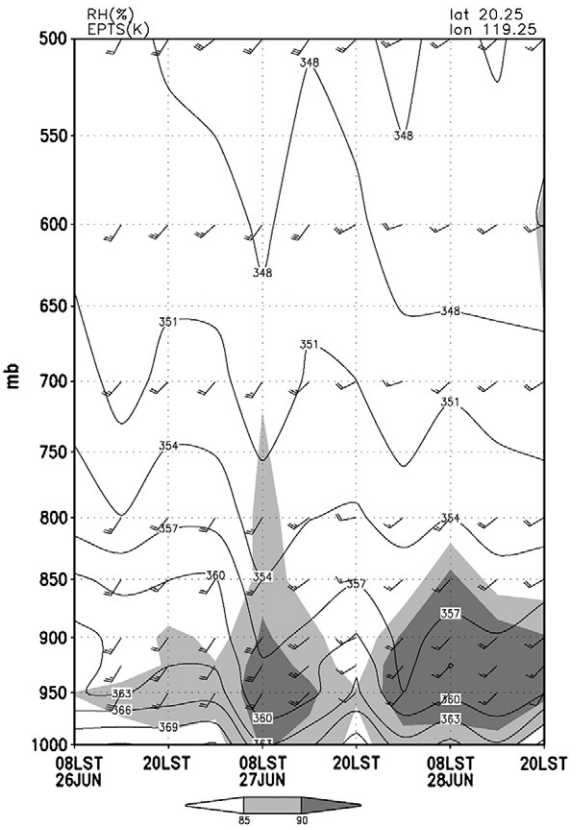

Fig. 5. The temporal variation of the profiles of wind, saturated equivalent potential temperature (contour interval is 3 °K), and relative humidity (greater than 90% in dark, between 90% and 85% in gray, less than 85% in white) over the northeast South China Sea at 20.25°N and 119.25°E during the period of 0800 LST 26 June to 2000 LST 28 June.

the high rainfall on June 27 and 28, 2008. In order to better resolve the orographic effects on the production of rainfall over Taiwan, nested grids with horizontal grid spacing of 27 km, 9 km, and 3 km were used at. All domains were comprised of 31 vertical levels from the surface to 50 hPa. The moisture processes included the subgrid-scale convective parameterization of Grell (1993) in Domains 1 and 2 and the grid-resolvable WSM 6-class microphysics scheme (Hong and Lim, 2006). Planetary boundary layer processes were represented by the Yonsei University PBL parameterization (Hong et al., 2006). The model was initialized and lateral boundary conditions derived from the ECMWF/TOGA analyses at 0800 LST (0000 UTC) 26 June 2008 and integrated for 66 h. In order to examine the orographic effects on the occurrence of the heavy rainfall over southwestern Taiwan, we performed a sensitivity test without Taiwan's topography (here after abbreviated as NT) on 9 and 3-km grid spacing simulations, while keeping everything else identical to the control run. The procedure of the setup of topography in the NT was similar to that in Chiao et al. (2004). In order to investigate the effect of cool air on the enhancement of rainfall over lowlands of southwestern Taiwan, a sensitivity experiment without the evaporation of raindrops (hereafter abbreviated as NEV) was performed.

3.2. Simulations of large-scale flow and the evolution of convection over the northeastern South China Sea on 27 and 28 June

After 0500 LST 27 June, the upper-level divergence over the northeastern South China Sea becomes evident which is caused by the increase of easterly winds from Bashi Channel to the northeastern South China Sea. The increase of easterly winds resulted from the westward-extension of the western Pacific subtropical high as illustrated at 300 hPa level at

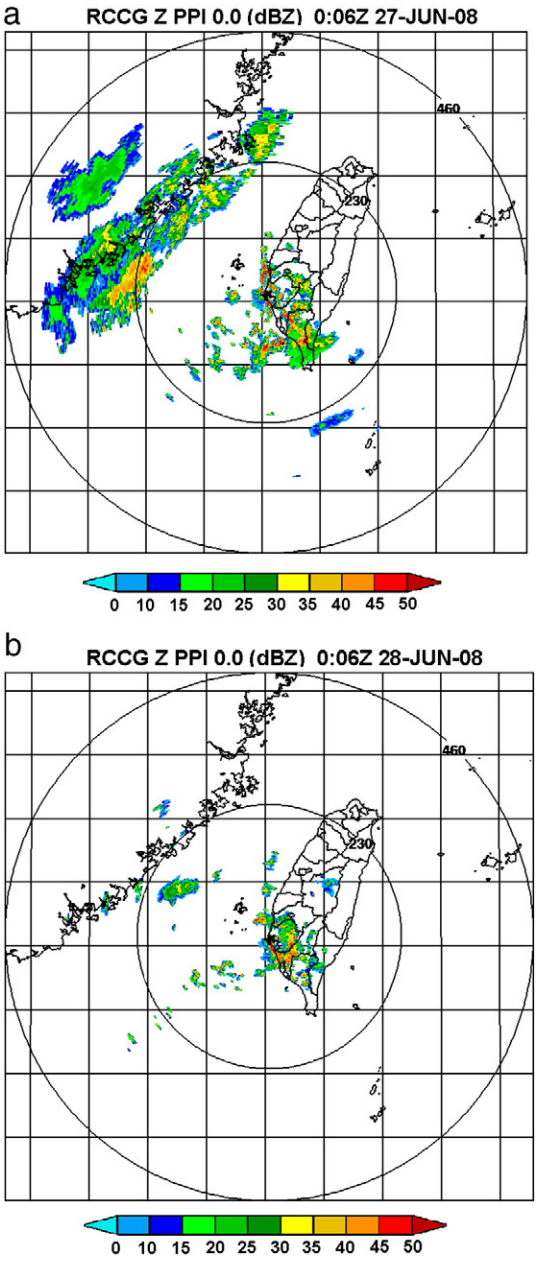

Fig. 6. (a) The maximum radar reflectivity in a vertical column of Chigu radar of Central Weather Bureau at 0806 LST 27 June 2008. The magnitude of reflectivity is denoted by the color scale in dBZ. (b) Same as (a) but for 0806 LST 28 June.

0800 LST (Hsu, 2010). The simulated upper-level divergence over the northeastern South China Sea is more pronounced than that observed (Fig. 4a). Meanwhile, the 300 hPa simulated trough moves eastward as observed (Fig. 4a).

The simulated upper-level divergence over the northeastern South China Sea disappears during the evening of 27 June and in the early morning of 28 June (not shown). At 0800 LST 28 June, a 300 hPa simulated trough over the central China on 27 June migrates slightly eastward as observed (Hsu, 2010) and the intensity of the western Pacific subtropical high also increases from that at 0500 LST. Meanwhile, the divergence over northeastern South China Sea and southern Taiwan Strait is caused by the change of the relatively slow easterly wind over Bashi Channel to a relatively faster southeasterly or southerly wind over Taiwan Strait (Hsu, 2010).

In order to investigate formation of convective activity over the northeastern South China Sea in the early morning of 27 June as indicated by the observations (Fig. 6), the simulation results from the 9 km grid spacing simulation is performed. At 0500 LST 27 June, beneath the upper-level convergence over the northeastern South China Sea (not shown), there is a lack of convective activity and low-level upward motion over the northeastern South China Sea, consistent with the observed radar echoes at 0500 LST (not

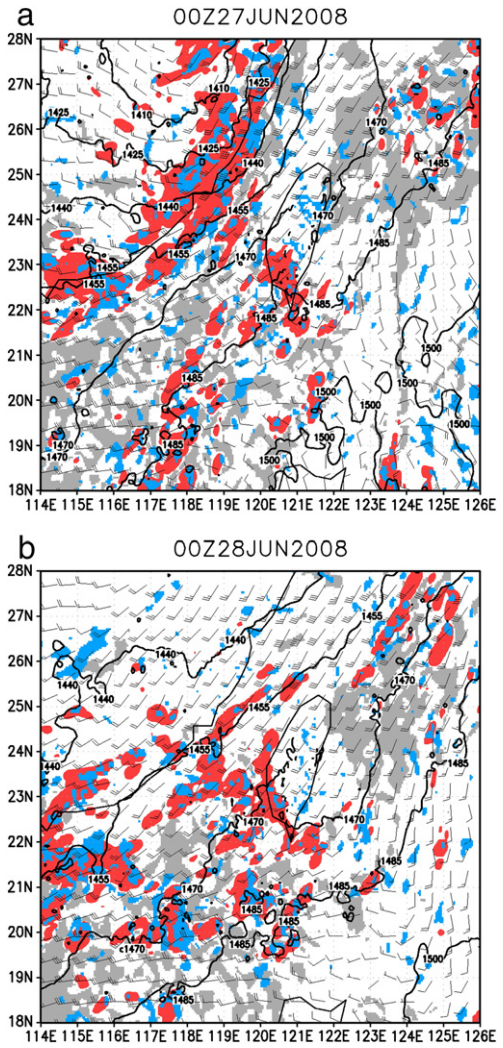

Fig. 7. (a) The simulated 850 hPa heights (solid lines, 15 gpm contour interval) and winds at 0800 LST 27 June 2008 in the 9 km grid spacing simulation. The blue areas represent the ascending motion exceeding 0.1 m s^{-1} at 500 hPa. The gray areas denote the mixing ratio of water vapor exceeding 17 g kg^{-1} at 925 hPa. The red areas denote the rainfall rate exceeding 1 mm h^{-1}. (b) Same as (a) but for 28 June.

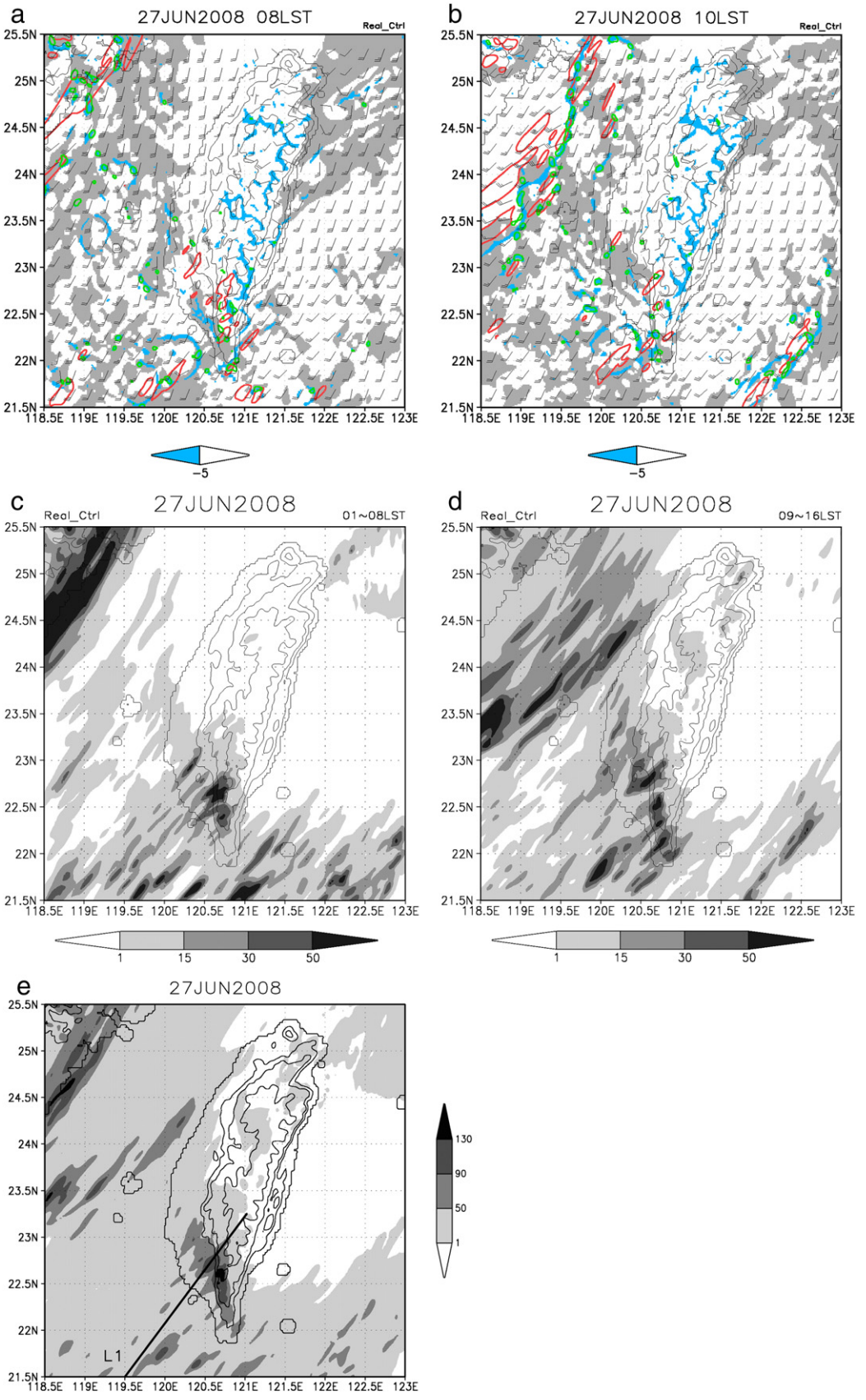
a
27JUN2008 08LST
Real_Ctrl
b
27JUN2008 10LST
Real_Ctrl
25.5N
25N
24.5N
24N
23.5N
23N
22.5N
22N
21.5N
118.5E 119E 119.5E 120E 120.5E 121E 121.5E 122E 122.5E 123E
−5
c
27JUN2008
Real_Ctrl
01~08LST
d
27JUN2008
Real_Ctrl
09~16LST
1 15 30 50
e
27JUN2008
130
90
50
1
L1

shown). At 0800 LST, the simulated convection (indicated by the 500 hPa ascending motion and surface rainfall), embedded in the moist airstream shown by 925 hPa moisture, intensifies as it moved toward southwestern Taiwan (Fig. 7a) beneath the upper-level divergence areas. This is consistent with the development of the observed radar echoes at 0800 LST (Fig. 6a). In a few hours, the area of convective activity moves inland and produces heavy rainfall over southwestern Taiwan as will be discussed in Section 3.3. The convective activity over the northeastern South China Sea weakens in the evening (not shown) as the upper-level divergence disappears and the low-level moisture decreases (Fig. 5).

In the morning of 28 June, beneath the upper-level divergence, the simulated convection develops over the ocean near the northeastern South China Sea and southern Taiwan Strait (Fig. 7b) as shown in radar echoes (Fig. 6b). Over the lowlands of southwestern Taiwan, convection also appears (Fig. 7b), which is consistent with observations (Fig. 6b). The simulated convective activity, embedded in the moist airstream, becomes very strong over the ocean near southwestern Taiwan and the lowlands of southwestern Taiwan at and after 0800 LST and produces heavy rainfall as will be shown in the next section (Section 3.3).

3.3. The simulated rainfall over southwestern Taiwan

In order to investigate the convective activity when it arrives at coastal areas of southwest Taiwan, the results simulated by the nested domain employing a 3-km grid spacing will be used. In the morning of 27 June, some of the convection (indicated by 850 hPa ascending motion and surface rainfall) over the nearby ocean moves inland toward southwestern Taiwan (Fig. 8a and b), and produces heavy rainfall over slope areas. The convective system continues to move inland from the nearby ocean into southwestern Taiwan and then becomes enhanced along the sloped areas thus producing heavy rainfall in southern Taiwan on 27 June (Fig. 8c and d). The accumulated rainfall during the periods of 0100 to 0800 LST and 0900 to 1600 LST (Fig. 8c and d) is qualitatively similar to the observed (Fig. 2a and b). The inland-movement of convection weakens in the evening (Section 3.2) resulting in lighter rainfall in southern Taiwan (not shown). In the lowlands near coastal areas of southwestern Taiwan, no heavy rainfall is simulated as was in the sloped areas (Fig. 8e). The accumulated daily rainfall shows that a maximum rainfall of 185 mm over the sloped areas occurs (Fig. 8e), slightly less than that observed (Fig. 2c).

In the morning of 28 June, the prevailing southwesterly wind occurs over southwest coast (Fig. 9a) and an easterly flow appears in the lowlands near 23°N as observed (Fig. 3d). Meanwhile, some convective cells develop over the ocean near southwestern Taiwan, which were embedded in the moist flow (Fig. 7b) followed by rainfall which appeared in the nearby ocean and lowlands of southwestern Taiwan (Fig. 9a). Rainfall over the lowlands in southwestern Taiwan persists until afternoon (Fig. 9b) as the convection continues moving into southwestern Taiwan. The simulated accumulated rainfall from 0100 to 0800 LST, 0900 to 1600 LST, and daily accumulated rainfall on 28 July (Fig. 9c–e) indicate that rainfall develops over the lowlands of southwestern Taiwan similar to that observed (Fig. 3). The maximum simulated daily rainfall is 198 mm (Fig. 9e), which is about 36 mm higher than observed in the lowlands (Fig. 3c). The simulated rainfall over the slopes areas on 28 June, however, is much higher than that observed (Fig. 3c).

4. Mechanisms of formation and maintenance for the localized heavy rainfall episode

The generation of heavy rainfall along the slopes on 27 June is illustrated by a temporal evolution of the simulated rainfall (Fig. 10a) along a northeast–southwest oriented cross section L1 passing through the high rainfall area (Fig. 8e). In the early morning, before the arrival of the inland-movement of the convective system (indicated by the ascending motion at the 980 hPa level and surface rainfall) from the nearby ocean, rainfall is generated over the slopes due to the lifting of moist air (not shown). During the periods of 0600–0800 LST and 0900–1030 LST, when the convective activity from the nearby ocean arrives (Fig. 10a), the rainfall over the mountain slopes is enhanced by conditional instability as illustrated by convective cell A at 0730 LST (Fig. 10b). In addition, rainfall occurs over the lowlands near the foothill where cool air is distinct (Fig. 10a). For example, when cell A decays over the mountain at 0830 LST, cell B appears near the cool air area in the lowlands (Fig. 10a and c). When cell B arrives at the foothill, cell C forms near the cool air area in the lowlands as the inland-movement convection is distinct (Fig. 10a and d). When cell C moves to the foothill, cell D commences in the lowlands near the cool air area (Fig. 10a and e). Several cells form associated with cool air over the lowlands in the upstream side of the old cells and then intensifies while moving toward sloped areas in the morning of 27 June resulting in high accumulated rainfall near the foothill (Fig. 8e and 10a). The evolution of convective cells during 0800 to 1000 LST is similar to the convection embedded in the flow Regime I found by Chu and Lin (2000). Note that Regime I of Chu and Lin is characterized by upstream propagation of the convective system and, in the mean time, the downstream propagation of the individual convective cell. The convection over the nearby ocean is weaker than the convection over the

Fig. 8. (a) The simulated surface winds, convergence, and rainfall rate in the 3 km grid spacing simulation at 0800 LST 27 June 2008. The gray areas represent the mixing ratio of water vapor greater than 17 g kg^{-1} at 925 hPa. The red lines enclose the areas with rainfall rate exceeding 10 mm h^{-1}. The blue areas represent the surface convergence greater than 5×10^{-4} s^{-1}. The green areas denote the ascending motion exceeding 0.1 m s^{-1} at 850 hPa. Terrain height (solid lines) is 200, 500, and 1500 m, respectively. (b) Same as (a) but for 1000 LST 27 June. (c) The simulated accumulated rainfall from 0100 to 0800 LST 27 June. The magnitude of the accumulated rain is shown by the gray scale in mm. Terrain height (solid lines) is 200, 500, and 1500 m, respectively. (d) Same as (c) but for the interval from 0900 to 1600 LST 27 June. (e) The magnitude of accumulated 24 h rainfall starting at 0000 LST on 27 June is shown by the gray scale in mm. Terrain height (solid lines) is 200, 500, and 1500 m, respectively. Line L1 is used in Fig. 10.

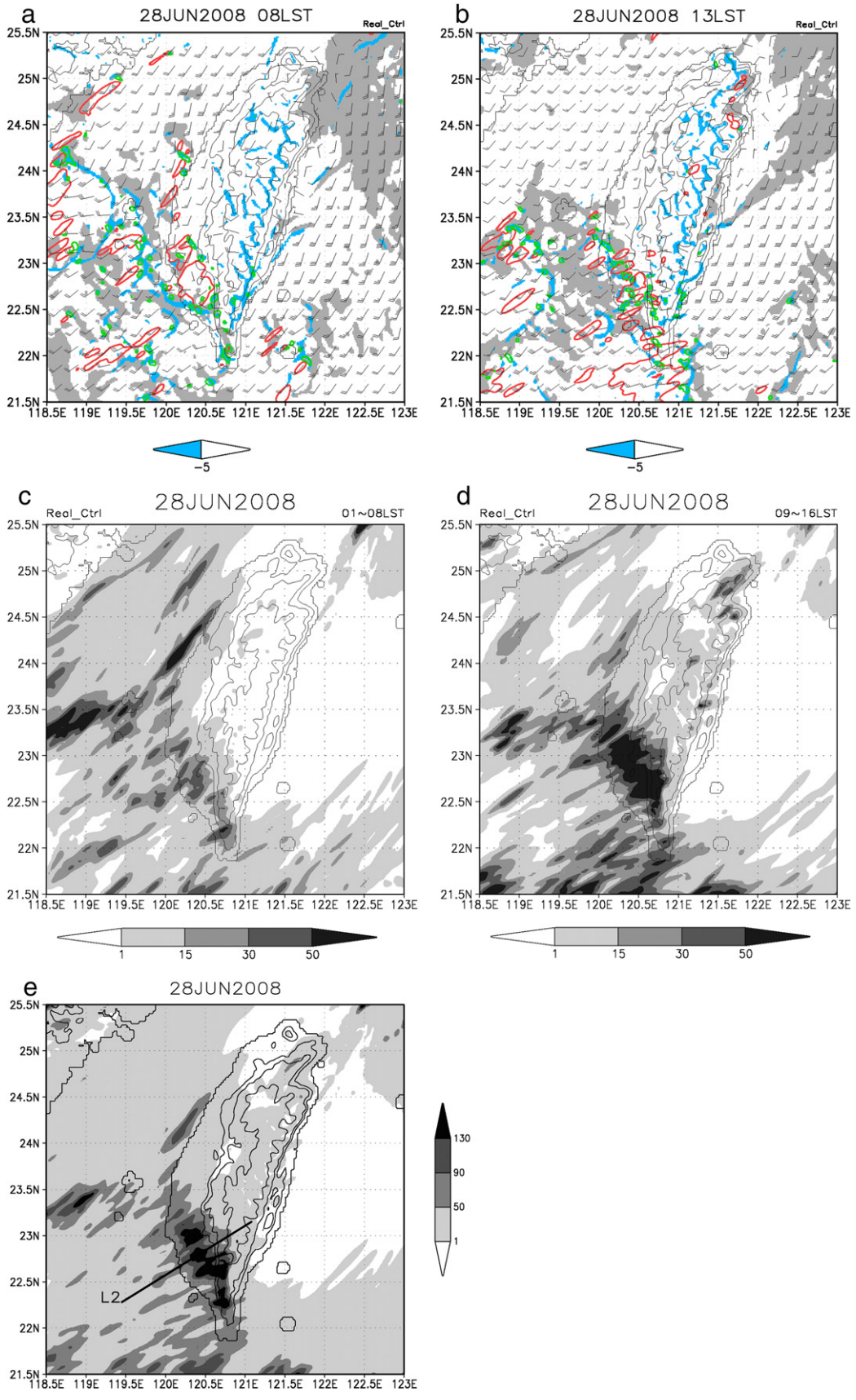
a
28JUN2008 08LST
Real_Ctrl
b
28JUN2008 13LST
Real_Ctrl
25.5N
25N
24.5N
24N
23.5N
23N
22.5N
22N
21.5N
118.5E 119E 119.5E 120E 120.5E 121E 121.5E 122E 122.5E 123E
-5
c
28JUN2008
Real_Ctrl
01~08LST
d
28JUN2008
Real_Ctrl
09~16LST
1 15 30 50
e
28JUN2008
L2
130
90
50
1

mountain slopes. The simulation results clearly indicate that the orographic effects and cool air generate strong convection and maintain localized heavy rainfall over the slopes.

On 28 June, the convergence areas over the southwestern lowlands occur frequently (Figs. 9a and 11a) due to the interaction between the prevailing southwesterly airstream and the deflected southeasterly flows in a low-Fr regime (Section 2). In addition, cool air produced by evaporation over the sloped areas also enhances rainfall over the coastal areas (Fig. 11a) as shown in an east–west oriented cross section L3 (Fig. 11b) passing southwestern Taiwan in Fig. 11a, where heavy accumulated rainfall is simulated (Fig. 9e). Notice that the southeasterly flow extends to the southwest coast (Fig. 11a) and up to 950 hPa over the lowlands and coastal areas (Fig. 11b). Low-level offshore flow associated with the southwesterly flow which is deflected from the prevailing wind by the CMR and enhanced by cool air interacts with the prevailing winds near the coastal area and enhances the development of convection over the lowlands. Coastal rainfall enhancement by offshore/land-breeze over southwestern Taiwan in the early morning during Mei-Yu (16 May–15 June) and summer rainfall regime (16 July–31 August) is also proposed by Kerns et al. (2010). The persistent rainfall and the associated ascending motion over the lowlands and coastal areas of southwestern Taiwan is illustrated by the temporal evolution of simulated rainfall (Fig. 11c) along a northeast–southwest oriented line L2 passing through the high accumulated rainfall over southwest Taiwan (Fig. 9e). Fig. 11c shows that the continuous inland-movement of the convective system from the nearby ocean to the lowlands from 0500 to 1200 LST of 28 June is enhanced over coastal areas and the lowlands over convergence areas (Figs. 9a and 11a). The enhancement of rainfall over the lowlands results in a heavier rainfall over the lowlands than the slopes (Fig. 9e).

5. The sensitivity tests

In order to test the influence of the Taiwan topography on the localized heavy rainfall, an experiment NT is performed. The absence of topography produces no orographic lifting over sloped areas and no flow confluence over the lowlands in NT (not shown). The accumulated rainfall (Fig. 12) shows that the rainfall stretches from the nearby ocean to southwestern Taiwan. Unlike the control run (Figs. 8e and 9e), the rainfall maximum over southwestern Taiwan is absent in NT (Fig. 12).

In order to examine the enhancement of low-level convergence due to cool air, an NEV experiment is performed. At 0700 LST on June 28, southeasterly flow is over the lowlands of southwestern Taiwan in NEV (Fig. 13a) due to orographic effects similar to that of the control run (Fig. 11a). However, weaker and shallower easterly wind along an east–west oriented cross section L4 (Fig. 13a) near the coastal area in NEV (Fig. 13b) relative to that in the control run (Fig. 11b) interacts with the prevailing wind to produces weaker convection over the coasts in NEV (Fig. 13b) relative to that in the control run (Fig. 11b). As a result, the weaker convection near coastal area produces less accumulated rainfall over lowlands in NEV (Fig. 13c) than in the control run (Fig. 9e).

The simulation results indicate that the orographic lifting due to strong winds contributes to high accumulated rainfall over the slopes on June 27. The strong lifting due to stronger incoming flow can be explained by $w \cong U\partial h/\partial x$, where w is the vertical velocity, U the incoming basic wind velocity, and h the mountain height profile (Lin et al., 2001; Lin, 2007). On the next day, the low-level convergence over the lowlands resulting from the confluence of flow due to flow deflection over southern Taiwan and enhanced by cool air from sloped areas produces high accumulated rainfall over the lowlands during the June 28 episode.

6. Summary

The occurrences of localized heavy rainfall events on 27 June 2008 are examined based on the analysis of ECMWF gridded data, satellite imagery, radar reflectivity, ARMTS rainfall data, and WRF model simulations. The analysis of the observed data on 27 and 28 June indicates that convection over the nearby ocean next to southwestern Taiwan moves toward Taiwan beneath no distinct upper-level divergence.

The simulated convection over the nearby ocean of southwestern Taiwan becomes active when the simulated upper-level divergence occurs over the southern Taiwan Strait and northeastern South China Sea. It is found that the conditional instability is released over sloped areas by orographic lifting of the moist air and convection on 27 June. The continuous inland-movement convection embedded in the relatively faster moist southwesterly flow, which is consistent with the observed convection, ascends over southwestern sloped areas thus maintaining the development of heavy rainfall over sloped areas. Near the foothills of southwestern sloped areas, the cool air associated with convection over sloped areas help the convection to develop over the lowlands and produced heavy rainfall. The simulated rainfall pattern is similar to the observed. The newly formed convective cell is on the upstream side of the old cell over the sloped areas. The evolution of old and new convection is similar to the convection in Regime I proposed by Chu and Lin (2000), which is characterized by upstream propagation of the convective system and downstream propagation of individual convective cells. On 28 June, the existing convection embedded in a relatively slow moist southwesterly wind is strengthened over the low-level convergence areas near the lowlands and coasts of southwestern Taiwan due to the orographically deflected prevailing southwesterly flow. In addition, the cool air from the sloped areas enhances the offshore flow which interacts with the prevailing flow to strengthen the low-level convergence over the lowlands and coastal areas. As a result, heavy rainfall is produced and maintained over the lowlands near coastal area. If Taiwan's CMR is removed, no maximum accumulated rainfall over the southwestern region is produced by the inland-movement of convection because of the lack of orographic effects. Without the additional evaporative cooling associated

Fig. 9. (a) Same as Fig. 8a but for 28 June. (b) Same as Fig. 8b but for 1300 LST 28 June. (c) Same as Fig. 8c but for 28 June. (d) Same as Fig. 8d but for 28 June. (e) Same as Fig. 8e but for starting at 0000 LST 28 June. Line L2 is used in Fig. 11c.

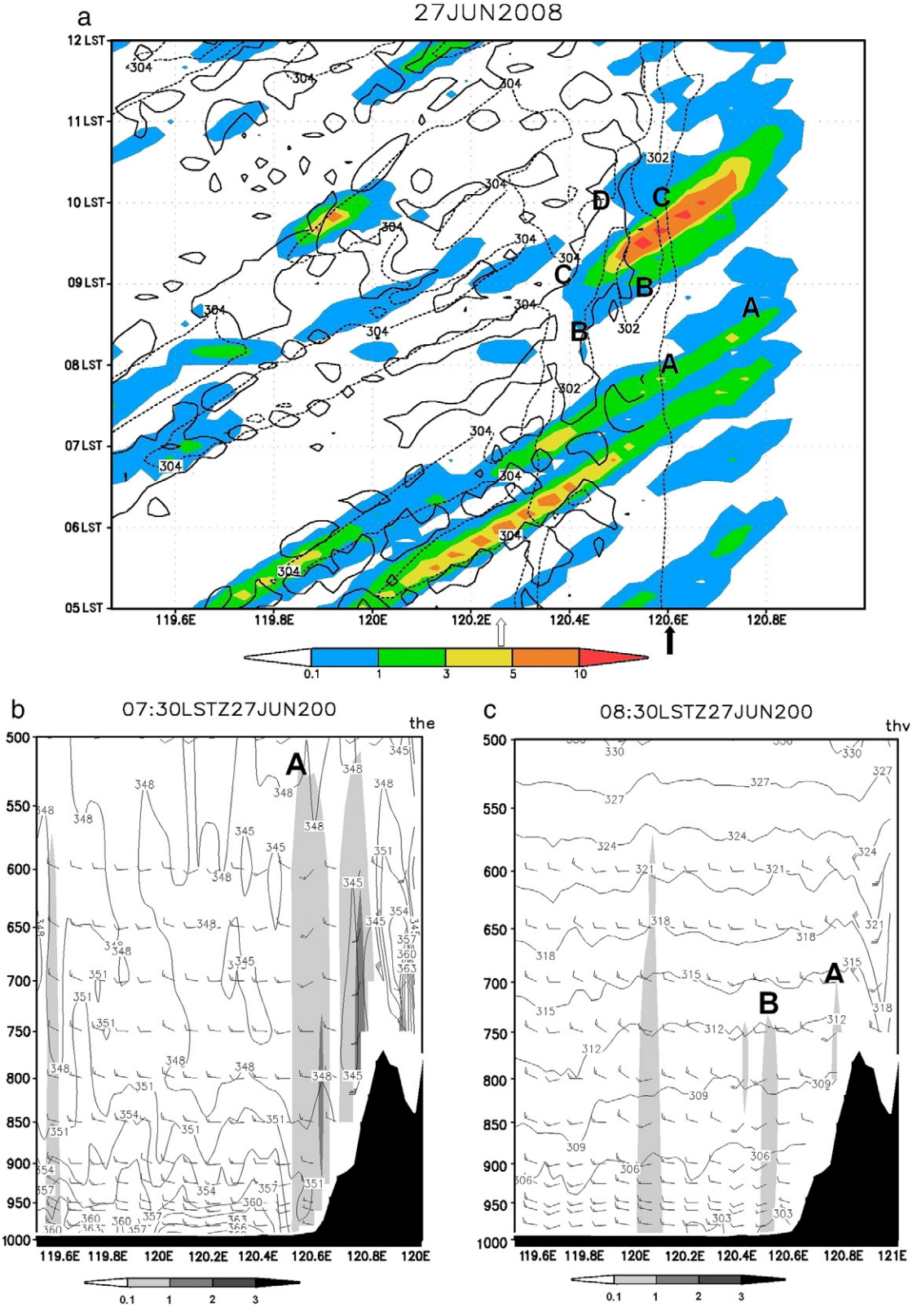
a
27JUN2008
12 LST
11 LST
10 LST
09 LST
08 LST
07 LST
06 LST
05 LST
119.6E
119.8E
120E
120.2E
120.4E
120.6E
120.8E
0.1
1
3
5
10
b
07:30LSTZ27JUN200
the
c
08:30LSTZ27JUN200
thv
A
B
C
D
119.6E 119.8E 120E 120.2E 120.4E 120.6E 120.8E 120E
119.6E 119.8E 120E 120.2E 120.4E 120.6E 120.8E 121E
0.1 1 2 3

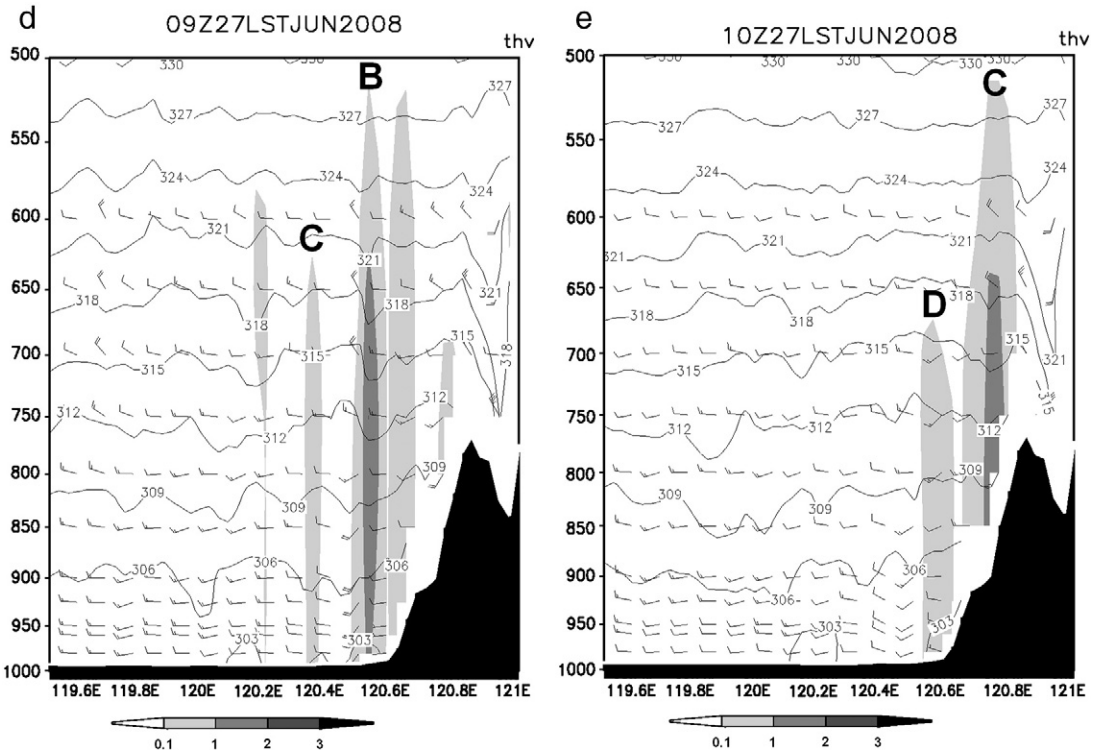

Fig. 10. (a) Temporal evolution of simulated rainfall along a northeast–southwest line L1 in Fig. 8e from the 3-km grid spacing simulation during 0500–1200 LST on 27 June 2008. Intensity of rainfall rate during a 10-min interval is shown by the color scale in mm. Solid lines enclose the areas with the ascending motion at 980 hPa exceeding 0.05 m s^{-1}. Dashed lines depict surface virtual potential temperature at 300, 302, and 304 K. The open and filled arrows at the bottom of the figure represent the approximate location of coastal line and the 500 m terrain height, respectively. Letter A to D denote convective cell A to D. (b) A vertical cross section along line L1 (Fig. 8e) at 0730 LST 27 June for simulated saturated equivalent potential temperature (solid lines, 3 °K), rain water (color areas) and along cross section winds obtained from the 3-km grid spacing model in the control run. Smoothed terrain along line L1 is represented by the darkened area. The magnitude of rainfall water is shown by the gray scale in g kg^{-1}. Letter A denote cell A. (c) Same as (b) but for 830 LST. Solid lines represent virtual potential temperature (3 °K). Letter B denote cell B. (d) Same as (c) but for 0900 LST. Letter C denote cell C. (e) Same as (c) but for 1000 LST. Letter D denote cell D.

with precipitation, the accumulated rainfall over the lowlands near the coastal area on 28 June is less than that of the control run because of the absence of extra convergence caused by the interaction between the prevailing southwesterly flow and the southeasterly cool flow. The conclusion obtained in this study is based on a single case study. More heavy rainfall cases over southwestern Taiwan will be examined in the future to better explore the orographic effects on the formation of localized heavy rainfall over southwestern Taiwan. In addition, in removing the mountains from the ECMWF data (case NT) to initialize the WRF model, readers should keep in mind that some effects of implicit existence of the topography might exist in the model results due to the extrapolations of ECMWF data on the mountain surface and in the atmosphere into the region originally occupied by the mountains. This problem does put some limitations on the sensitivity experiment without Taiwan topography (case NT) and deserves a further study.

Acknowledgements

This work is supported by the National Science Council of Taiwan under Grant NSC 96-2111-M-008-018 and the NOAA Educational Partnership Program (EPP) under Cooperative Agreement NO: NA06OAR4810187. We thank the Central Weather Bureau, Taipei, Taiwan, for providing the data. The computer resources were supplied by the Center for Computational Geophysics, National Central University, Chung-Li, Taiwan.

References

Chen, C.-S., Chen, Y.-L., 2003. The rainfall characteristics of Taiwan. Mon. Wea. Rev. 131, 1323–1341.
Chen, Y.-L., Li, J., 1995. Large-scale conditions favorable for the development of heavy rainfall during TAMEX IOP 3. Mon. Wea. Rev. 123, 2978–3002.
Chen, C.-S., Chen, W.-C., Chen, Y.-L., Lin, P.-L., Lai, H.-C., 2005. Investigation of orographic effects on two heavy rainfall events over southwestern Taiwan during the Mei-yu season. Atmos. Res. 73, 101–130.
Chen, C.-S., Chen, Y.-L., Liu, C.-L., Lin, P.-L., Chen, W.-C., 2007. Statistics of heavy rainfall occurrences in Taiwan. Weather Forecasting 22, 981–1002.
Chen, C.-S., Lin, Y.-L., Peng, W.-C., Liu, C.-L., 2010a. Investigation of a heavy rainfall event over southwestern Taiwan associated with a subsynoptic cyclone during the 2003 Mei-Yu season. Atmos. Res. 95, 235–254.
Chen, C.-S., Liu, C.-L., Yen, M.-C., Chen, C.-Y., Lin, P.-Lang, Huang, C.-Y., Teng, J.-H., 2010b. Terrain effects on an afternoon heavy rainfall event, observed over northern Taiwan on 20 June 2000 during monsoon break. J. Meteorol. Soc. Jpn. 88, 649–671.
Chiao, S., Lin, Y.-L., Kaplan, M.L., 2004. Numerical study of the orographic forcing of heavy precipitation during MAP IOP-2B. Mon. Wea. Rev. 132, 2184–2203.

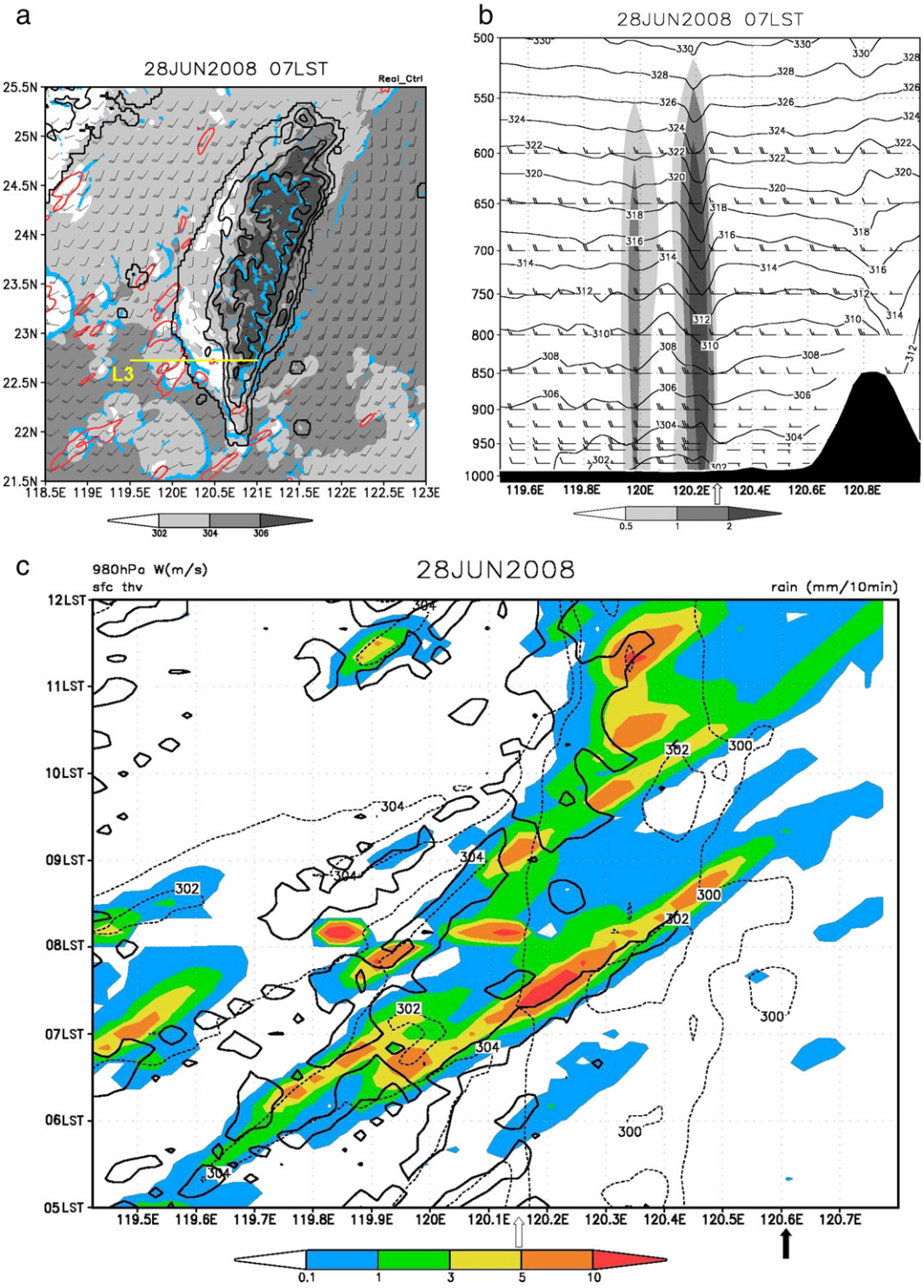

Fig. 11. (a) The simulated surface winds, virtual potential temperature, rainfall rates and convergence from the 3-km grid spacing model domain at 0700 LST on 28 June. The rainfall rate exceeding 10 mm h^{-1} is enclosed by red lines. The blue areas denote the surface convergence exceeding 5×10^{-4} s^{-1}. The magnitude of virtual potential temperature is denoted by gray scale (K). Terrain height contours (solid lines) are 200, 500, and 1500 m, respectively. The east–west oriented line L3 is used in Fig. 11b. (b) A vertical cross section along line L3 (Fig. 11a) at 0700 LST 27 June for simulated virtual potential temperature (solid lines, K), rain water (shaded areas in g kg^{-1}) and along cross section winds obtained from the 3-km grid spacing model domain in the control run. Smoothed terrain along line L3 is darkened. The open arrow represents the approximate location of coastal line. The magnitude of rain water is shown by the gray scale in g kg^{-1}. (c) Same as Fig. 10a but for line L2 during 0500 to 1200 LST on 28 June.

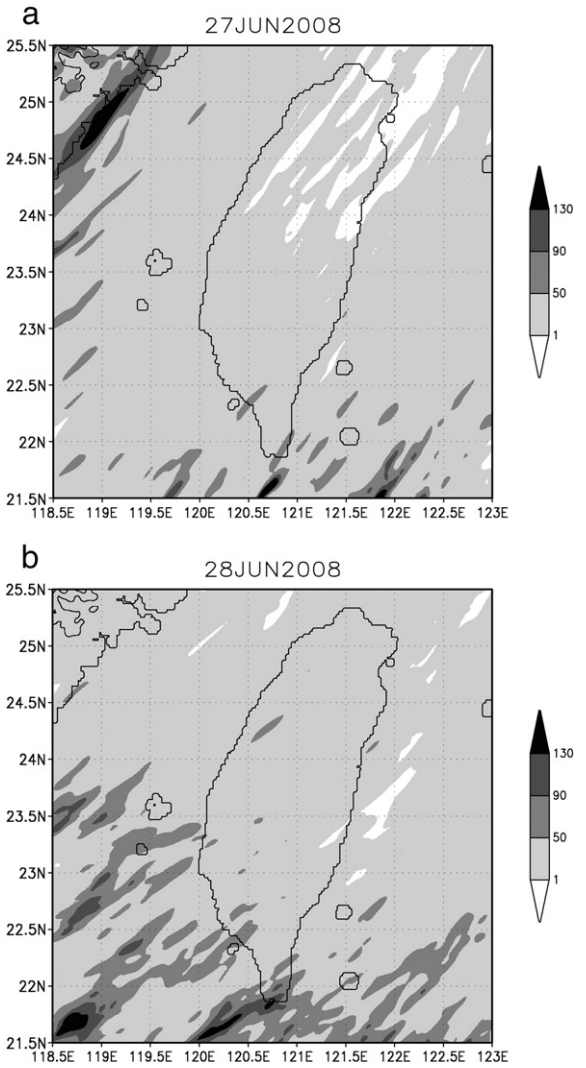

Fig. 12. (a) Same as Fig. 8e but for NT sensitivity experiment. (b) Same as Fig. 9e but for NT sensitivity experiment.

Chu, C.-M., Lin, Y.-L., 2000. Effects of orography on the generation and propagation of mesoscale convective systems in a two-dimensional conditionally unstable flow. J. Atmos. Sci. 37, 3817–3837.

Federico, S., Avolio, E., Pasqualoni, L., De Leo, L., Sempreviva, A.M., Bellecci, C., 2009. Preliminary results of a 30-year daily rainfall data base in southern Italy. Atmos. Res. 94, 641–651.

Grell, G.A., 1993. Prognostic evaluation of assumptions used by cumulus parameterization. Mon. Wea. Rev. 121, 764–787.

Hong, S.-Y., Lim, J.-O.J., 2006. The WRF single-moment 6-class microphysics scheme (WSM6). J. Korean Meteorol. Soc. 42, 129–151.

Hong, S.-Y., Noh, Y., Dudhia, J., 2006. A new vertical diffusion package with an explicit treatment of entrainment processes. Mon. Wea. Rev. 134, 2318–2341.

Hsu, N.-N., 2010. A preliminary study of orographic effects on localized heavy rainfall events over southwestern Taiwan during 27–28 June 2008. MS thesis (In Chinese), NCU, Chung-Li, Taiwan, 99 pp.

Hunt, C.R., Snyder, W.H., 1980. Experiments on stably and neutrally stratified flow over a model three-dimensional hill. J. Fluid Mech. 96, 671–704.

Kerns, B.W.J., Chen, Y.-L., Chang, M.-Y., 2010. The diurnal cycle of winds, rain, and clouds over Taiwan during the Mei-Yu, summer, and autumn rainfall regimes. Mon. Wea. Rev. 138, 4261–4275.

Lin, Y.-L., 2007. Mesoscale Dynamics. Cambridge University Press, New York. 630 pp.

Lin, Y.-L., Chiao, S., Wang, T.-A., Kaplan, M.L., Weglarz, R.P., 2001. Some common ingredients for heavy orographic rainfall. Weather Forecasting 16, 633–660.

Mastrangelo, D., Horvath, K., Riccio A, Miglietta, M.M., in press. Mechanisms for convection development in a long-lasting heavy precipitation event over southeastern Italy. *Atmos. Res.*

Skamarock, W.C., Klemp, J.B., Dudhia, J., Gill, D.O., Barker, D.M., Wang, W., Powers, G., 2005. A description of the Advanced Research WRF version 2. NCAR Tech. Note TN-468 + STR. 88 pp. [Available from NCAR, P.O. Box 3000, Boulder, CO 80307].

Sow, K.S., Juneng, L., Tangang, F.T., Hussin, A.G., Mahmud, M., 2011. Numerical simulation of a severe late afternoon thunderstorm over Peninsular Malaysia. Atmos. Res. 99, 248–262.

Wang, S.-T., Cheng, H., Shu, C.-H., Chao, Y.-K., 1985. The environmental condition for heavy rainfall in Taiwan during May and June. Proc. Conf. on Weather Analysis and Forecasting. Central Weather Bureau, Taipei, Taiwan, pp. 55–88.

Xu, W., Zipser, E.J., Liu, C., 2009. Rainfall characteristics and convective properties of Mei-Yu precipitation systems over south China, Taiwan, and the South China Sea. Part I: TRMM observations. Mon. Wea. Rev. 137, 4261–4275.

Yen, M.-C., Chen, C.-C., Hu, H.-L., Tzeng, R.-Y., Dinh, D.T., Nguyen, T.T.T., 2011. Interannual variation of the fall rainfall in central Vietnam. J. Meteorol. Soc. Jpn. 89, 259–270.

Zhang, Q.-H., Lau, K.-H., Kuo, Y.-H., Chen, S.-J., 2003. A numerical study of a mesoscale convective system over the Taiwan Strait. Mon. Wea. Rev. 131, 1150–1170.

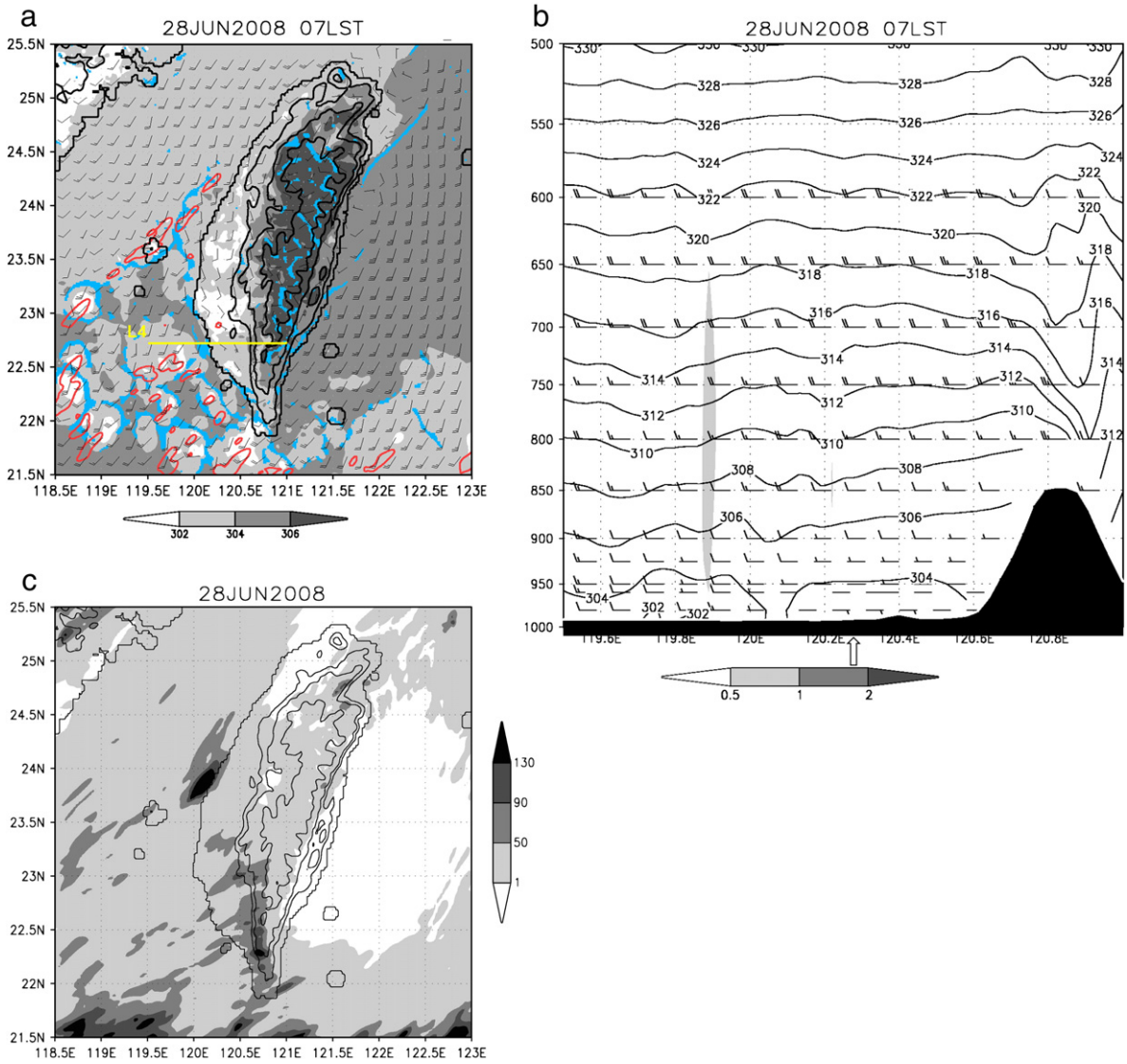

Fig. 13. (a) Same as Fig. 11a but for NEV sensitivity experiment. The east–west oriented line L4 is used in Fig. 13b. (b) Same as Fig. 11b but for a vertical cross section along L4 (Fig. 13a) for NEV sensitivity experiment. (c) Same as Fig. 9e but starting at 0000 LST 28 June for NEV sensitivity experiment.